Received: 17 April 2021 | Revised: 13 December 2021 | Accepted: 14 December 2021

DOI: 10.1002/iroh.202102096

RESEARCH PAPER

International Review of Hydrobiology

Wake flow patterns and turbulence around naturally deposited and installed trees in a gravel bed river

Ingo Schnauder[1,2] | Christine Anlanger[3] | Katinka Koll[4]

[1]Department of Hydraulic Engineering, Institute of Hydraulic Engineering and Water Resources Management, TU Wien, Vienna, Austria

[2]Gerstgraser—Ingenieurbüro für Renaturierung, Cottbus, Germany

[3]Department of River Ecology, Helmholtz Centre for Environmental Research - UFZ, Magdeburg, Germany

[4]Division for Hydraulic Engineering and River Morphology, Leichtweiß-Institute for Hydraulic Engineering and Water Resources, Technische Universität Braunschweig, Braunschweig, Germany

Correspondence
Ingo Schnauder, Department of Hydraulic Engineering, Institute of Hydraulic Engineering and Water Resources Management, TU Wien, Karlsplatz 13/222, Vienna 1040, Austria.
Email: ingo.schnauder@tuwien.ac.at

Handling Editor: Elisabeth Bondar-Kunze

Funding information
Bundesministerium für Bildung und Forschung, Grant/Award Number: 01LC1322F; Bundesministerium für Umwelt, Naturschutz und Reaktorsicherheit, Grant/Award Number: 01LC1322F; Bundesamt für Naturschutz, Grant/Award Number: 01LC1322F; Technische Universität Wien

Abstract

Large wood structures, such as wood fragments, debris jams, or entire trees, create flow and habitat diversity in rivers. A key flow feature associated with such structures is the wake, characterised by a core zone of reduced velocity and shear layers at its margins. Wakes are largely controlled by geometric and structural properties of the wood. In the present study, the flow patterns and turbulence created by different wood structures were compared at two study sites: naturally eroded and fragmented oaks (Site A) and artificial poplar installations (Site B). Flow and turbulence were quantified using pointwise velocity measurements with acoustic Doppler velocimeters (ADVs) and surface particle tracking velocimetry (SPTV). The measured flow patterns exhibited similarities with shallow porous wakes that feature fluid advection through the structure into the wake core downstream. Two additional features of wood structures were identified in the present study: (i) the growth of the shear layers was hindered by bed friction like for shallow mixing layers and (ii) the presence of a tree stem and sediment deposit in the wake centre delayed or even suppressed the interaction of the shear layers and vortex street formation similar to a wake-splitter plate. Methodologically, the combined ADV/SPTV measurement approach and the use of analytical models for shallow mixing layers proved to be highly valuable to decipher the complex flow patterns around wood structures in the field.

KEYWORDS
large wood, instream trees, root boles, wake flows

Abbreviations: ADV, acoustic Doppler velocimeter; GPS, global positioning system; HHQ, peak flow discharge; SL, shear layer; SPTV, surface particle tracking velocimetry; TKE, turbulent kinetic energy.

1 | INTRODUCTION

The first ground-breaking interdisciplinary research on large wood in rivers was carried out in the gravel bed river Tagliamento in Italy (Edwards et al., 1999; Gurnell et al., 2000). The Tagliamento research showed that deposited trees act as 'ecosystem engineers', creating unique habitat conditions and ecological functions on a scale much larger than the individual tree. With a focus on biogeomorphological processes, plant ecology and aquatic–terrestrial linkages, the local flow patterns around deposited trees and debris jams were not investigated (Schnauder & Moggridge, 2009). These local flow patterns, though, determine scouring and pool formation as well as the retention of fines which are the key mechanisms associated with ecosystem engineering.

The characteristic flow feature for most wood structures is the formation of a wake. Flow is diverted around the structure and then separates from it, creating a core zone of reduced mean velocity or even flow reversal. At the wake margins, shear layers evolve, driven by the velocity gradient between the slower wake zone and the faster ambient flow. Wake and shear layer characteristics depend largely on the structural properties of the wood configuration underlying a large heterogeneity and diversity in rivers. Therein, porosity is the only parameter studied systematically in open channel flows (Chang & Constantinescu, 2015; Nicolle & Eames, 2011; Prinz et al., 2012; Schnauder et al., 2007; Takemura & Tanaka, 2007; Zong & Nepf, 2012). In such idealised flume and numerical studies, porosity is conventionally approximated with group arrangements of vertical cylinders. Three main effects of cylinder-porosity were identified: (i) the near-wake is occupied by fluid that is advected through the cylinders and, thus, reduces the velocity difference between the wake centre and the ambient flow, (ii) two shear layers evolve at the wake margins but are less pronounced due to the decreased velocity difference and (iii) the shear layers are laterally separated by centrally advected fluid in the near-wake and do not interact until farther downstream, where a vortex street evolves for porosities that fall below a marginal value of 95% (Zong & Nepf, 2012).

Yet, these findings from cylinder configurations with vertical cylinders may not be directly transferable to wood in rivers featuring rather different structural properties. The present study gives the opportunity to quantify flow patterns around wood structures in a gravel bed river and to compare them with wake and shear flow types from the literature.

2 | ANALYTICAL MODELS FOR SHEAR LAYERS

Zong and Nepf (2012) formulated a relation for the wake length scale L_{KV} (m) downstream of the porous body where the shear layers begin to overlap and interact:

$$L_{KV} = \frac{D}{2\alpha}\frac{U_c}{\Delta U}, \tag{1}$$

where D is the patch width or diameter (m), α is the universal plane shear layer spreading coefficient (−) with a value in the range 0.11 ± 0.03, the centreline velocity $U_c = 0.5\,(U_1 + U_2)$ and the velocity difference $\Delta U = (U_2 - U_1)$. Herein, the wake velocity U_1 is determined by the porosity alone, whereas U_2 is the ambient flow velocity and equals the approaching velocity U_0 when the flow cross-section is wide enough to neglect blockage effects.

Because of the relatively short length of L_{KV} in their experiments, Zong and Nepf (2012) did not incorporate the destabilizing effect of bed friction on the shear layer growth (Chu & Babarutsi, 1988; Sukhodolov et al., 2010; Uijttewaal & Booij, 2000). In shallow flows, this effect is well represented by an exponential decrease of the growth in shear layer width δ (m) with increasing distance x' (m) from its origin (Van Prooijen, 2004):

$$\delta(x') = \delta_0 + \alpha\frac{\Delta U_0}{U_{c,0}}\frac{h}{c_f}\left(1 - \exp\left(-c_f\frac{x'}{h}\right)\right), \tag{2}$$

where δ_0 is the initial width (m), h is the water depth (m) and the bed friction coefficient $c_f = 2(u_*/U_0)^2$ calculated from the bed shear velocity u_*. The velocities $U_{c,0}$ and ΔU_0 are defined for the initial conditions ($x' = 0$). From the shear layer width, the dominant frequency of the local shear layer vorticity is calculated (Sukhodolov et al., 2010):

$$f_e(x') = \frac{1}{t_e(x')} \cong \frac{U_c}{\delta(x')}\left(\lambda^2\frac{2U_c}{c_f\Delta U}\right), \tag{3}$$

where λ is the empirical scaling coefficient (−), which relates the scale of the vortex structures to the shear layer width. It was determined to lie between 0.5 for weak shear layers with low velocity difference and 1.0 for a pronounced velocity difference, for example, in recirculating flows (Sukhodolov et al., 2010).

Shallow wake flows feature two shear layers that, in most cases, interact and form a vortex street behind the obstacle. For shallow wakes, the vortex shedding frequency was found for a universal Strouhal number of $St = 0.2$, independently of porosity and, thus, solely a function of patch width D in the investigated Reynolds-number range (Zong & Nepf, 2012):

$$St = \frac{f_{KV}D}{U_0} \cong 0.2 \quad \text{for} \quad 10^4 < Re_D = \frac{DU_0}{\upsilon} < 4 \times 10^4, \tag{4}$$

where υ is the kinematic viscosity (m²/s). The set of Equations (1)–(4) gives a theoretical framework for predicting flow patterns of wake flows and shear layers associated with porous structures in open-channel flows.

3 | FIELD SITES AND CONDITIONS

The Mulde River originates in the Ore Mountains at the German-Czech border and, after 125 km, joins the Elbe River near Dessau-Roßlau, Sachsen-Anhalt, Germany. Despite river regulations, the lower Mulde still features river bends with active bank erosion where

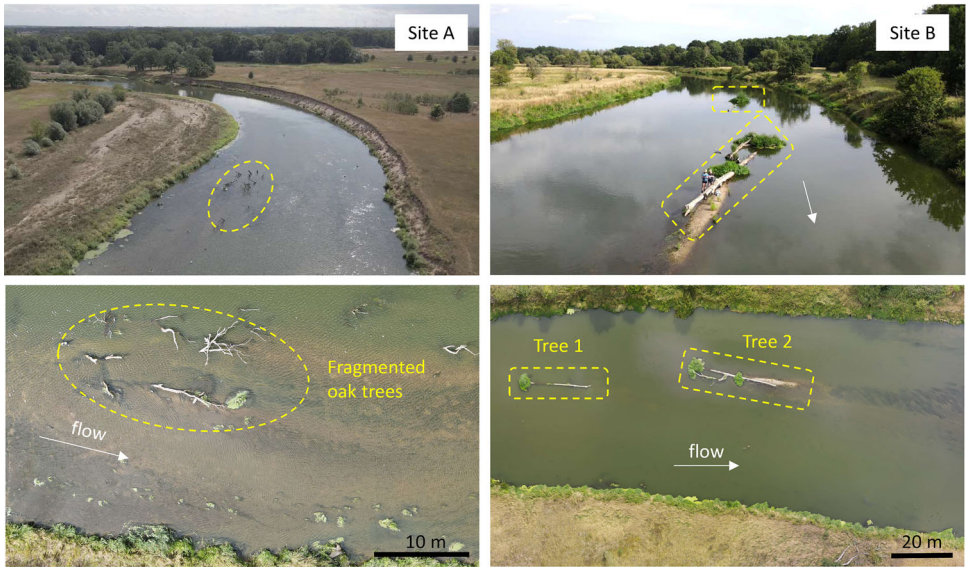

FIGURE 1 (a) Site A with naturally eroded, deposited and fragmented oaks. (b) Site B with the two installed poplars. Photos taken 2 years after installation with jammed debris and shrubby vegetation growing on the emergent root parts

trees are undercut and eroded. An example is Site A (51°46′14.06"N/12°17′49.05"E), where several large oak trees were eroded during the extreme flood in 2013 (HHQ = 1440 m^3/s). The oaks kept a stable position after deposition in the river but were subject to wear-off and fragmentation.

In comparison, Site B (51°47′59.19"N/12°16′7.76"E) has been subject to rigid bank protection (Figure 1b). Morphodynamics are limited to bed changes within the active cross-section. The site was, thus, suited for installing trees and monitoring hydraulic and morphologic changes and their effects on mesohabitats and biota (Schulz-Zunkel et al., 2022, this issue). For the tree installations at Site B, two nonnative hybrid poplars were cut nearby and anchored with steel chains to six concrete cubes of 1.0 m edge length (Anlanger et al., 2022, this issue). The two poplars were installed in a tandem configuration almost centrally in the river cross-section with a spacing of 25 m. The root bole was oriented upstream, facing the current, typical for trees deposited on floodplains (Gippel et al., 1996; Gurnell et al., 2002). During installation, the trees were cleared from side branches and smaller roots, leaving a root bole of 1.5 m diameter and a stem of 25 m length. The root bole structure was assumed to be impermeable to the flow (Figure S13). Algal blooms and poor visibility during the summer campaigns hindered a more detailed assessment or mapping of the root boles.

3.1 | Conditions during the measurement campaigns

Field campaigns were undertaken in the summers of 2018–2020, with pointwise flow measurements (ADV) across the water depth at Site A in 2018 and Site B in 2019. In 2020, surface flow velocity measurements (SPTV) were performed at both sites. Favourably, low flows of around 12 $m^3 s^{-1}$ occurred during all measurements and provided comparable hydraulic conditions. Spring flows between the campaigns were moderate at an elevated mean flow but below bankful discharge (see Figure S15 and further details in Schulz-Zunkel et al., 2022, this issue).

The oaks at Site A remained unchanged between the campaigns (Figure S14). At Site B, floating debris was trapped by the root boles. The efficient root bole diameter, thus, increased from 1.5 to 2.0 m until July 2019 and to 4.0 m until August 2020. Tree 2 further trapped a large wood fragment in 2020 and was slightly rotated in respect to the mean flow direction. SPTV measurements in 2020 were, therefore, only performed around the upstream tree (Tree 1).

Morphological changes and scouring likely occurred around the trees at Site A during the periods of increased discharge in spring 2019 and 2020. Their positive buoyancy may have floated the poplars, altering the flow from a wake to a jet-like underflow pattern and shifting the maximum scour position further downstream. However, as measurements are not available during the higher flows, field evidence is lacking.

4 | METHODS

4.1 | Pointwise flow measurements over the water depth

Time series of the three velocity components u, v, w (streamwise, lateral, vertical) were measured with two acoustic Doppler velocimeters (one downward looking field probe, one sideward looking lab probe installed in downward-looking position; ADV Nortek Vectrino+). The ADVs were installed on a vertically movable frame system that enabled precise horizontal alignment and vertical

positioning. Depending on the local water depth, three to six measurements were conducted in each vertical, with the lowest point 5 cm above the river bed and the highest point 5 or 12 cm below the water surface. The sampling time ranged from 150 s at Site A to 300 s at Site B, both taken at a sampling rate of 25 Hz. The orientation of the ADVs was measured with a standard compass, the global position with a GPS total station.

Post-processing of the ADV time series in ExploreV (Nortek AS) included the transformation to the local reference coordinate system and rotation of the measurement volume, standard filtering and spike-removal (Sukhodolov et al., 1998). Acoustic noise was well below 5% of the total turbulent kinetic energy (TKE) and required no further processing. Turbulent intensities, stresses, autocorrelations and autospectra were computed in ExploreV. Analyses in this study focused on the two dominant sources of shear: bed friction in the vertical and horizontal shear induced by the wake flow around the wood structures. Bed friction is parametrised by the shear velocity u_* (cm/s) and determined from a comparison with the theoretical boundary layer profiles of three parameters. Those included the log-law fit to velocity profiles in verticals $U(z)$ an exponential fit of turbulent intensity profiles [$u'(z)$, $v'(z)$, $w'(z)$] and TKE(z)] and a linear fit of turbulent stress profiles = $u'w'(z)$ (Nezu & Nakagawa, 1993). For identification of the horizontal shear layers, the maximum spanwise turbulent stresses = $u'v'$ (cm²/s²) in each vertical as well as the dominant periods or frequencies in the lateral velocity time series $v(t)$ were used. For a detailed description of the procedure, see the Supporting Information Material section.

Velocity and turbulence quantities are presented here in their dimensional form and not standardised by means of scaling parameters. As scaling requires defining fixed symmetries (e.g., two-dimensional or axially symmetric flows), this approach seemed more transparent and less subjective to misconceptions for the present superimposed flow structures.

4.2 | Surface flow velocities

To determine the surface flow patterns around the trees, SPTV was applied in summer 2020 using surface floaters. A few hundreds of thin starch discs with a diameter of 40 mm were added to the flow 10–20 m upstream of the trees. The bright discs contrasted well with the water and soaked up just enough not to be exposed to wind attack.

For the videos, a standard quadcopter (DJI Mavic Air 2) with a camera resolution of 12 megapixels at 30 frames/s hovered above the trees. The camera was oriented downward-looking, with the rotors and gimbal compensating for misalignments. However, movements due to strong and gusty winds were not fully compensated and required image stabilization in the post-processing of the videos. Fixed markers mounted on the trees served as anchor points for the image stabilization. The markers were georeferenced and further used for geometric scaling of the videos. Finally, the SPTV-analyses of the stabilised videos were performed in 'TracTrac' (Heyman, 2019).

4.3 | Water depth and grain size distribution

Bed elevations were determined from echosounder recordings with a georeferenced ADCP taken shortly before the flow measurements. At the locations of the ADV measurements, sediment samples were taken with a surface sampler and sieve analyses yielded local distributions of characteristic grain sizes of which d_{50} (mm) and the grain size standard deviation $\sigma = (d_{84}/d_{16})^{0.5}$ (–) were selected for comparison at both sites.

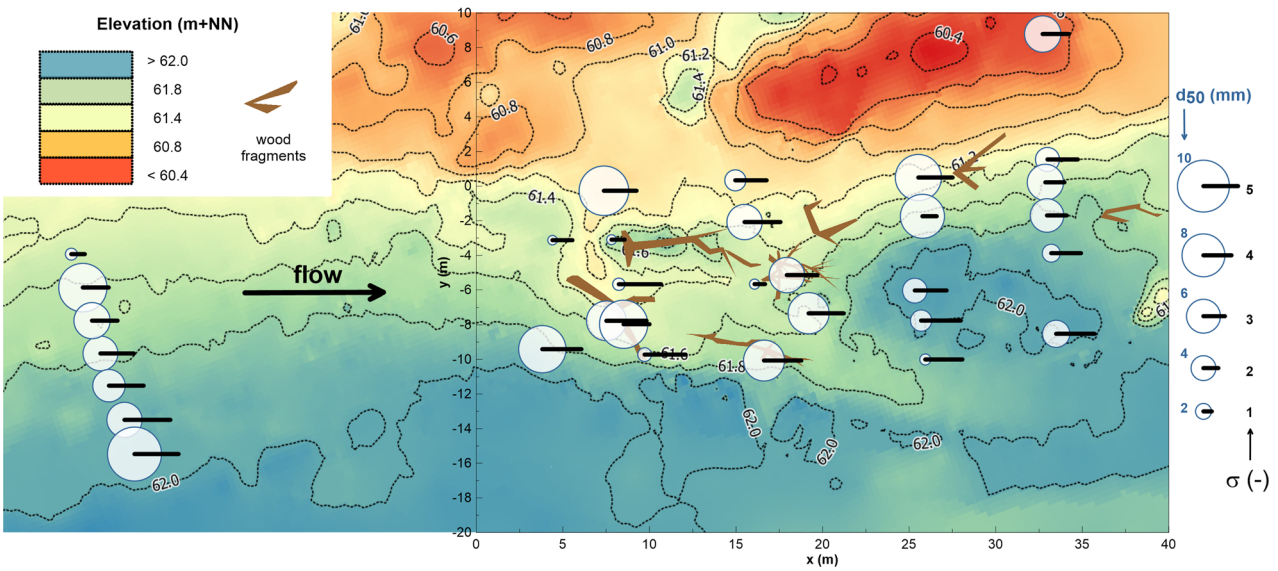

FIGURE 2 Contour plots of bed elevation at Site A from echosounder measurements. Circle size indicates grain size at the sediment sampling locations and black bars within the standard deviation

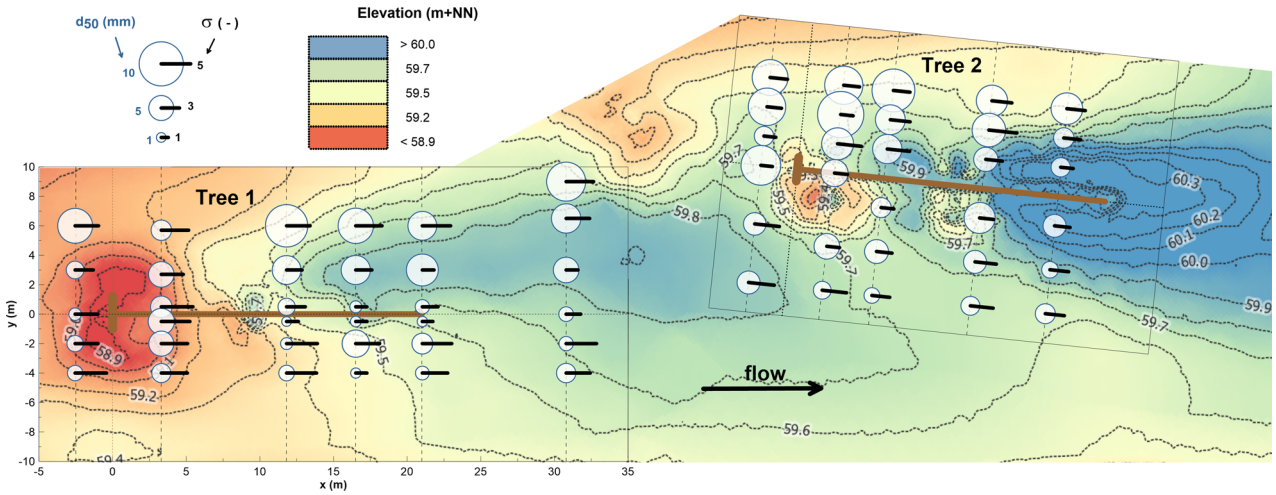

FIGURE 3 Contour plots of bed elevation at Site B from echosounder measurements; Circle size indicates grain size at the sediment sampling locations and black bars within the standard deviation

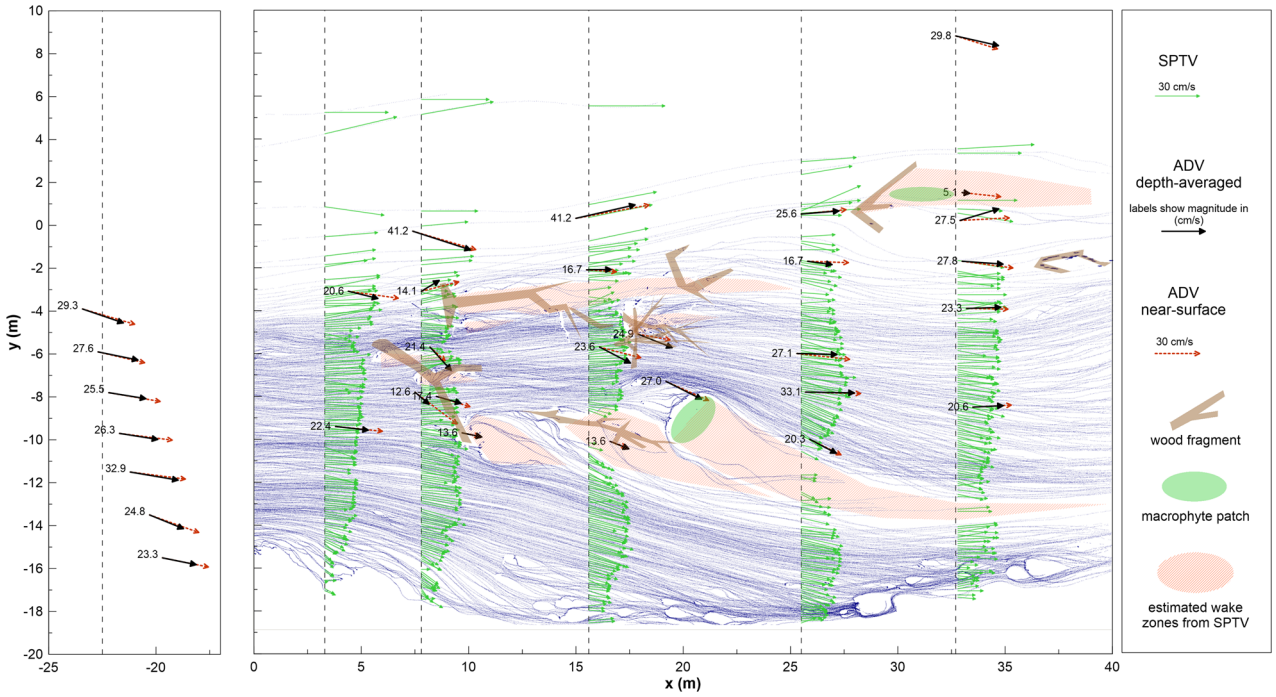

FIGURE 4 Vectors of horizontal mean flow velocity components (U, V) for the fragmented oaks at Site A. Acoustic doppler velocimeter (ADV) points contain depth-averaged and near-surface vectors measured 2018. Surface Particle Tracking Velocimetry (SPTV) velocity vectors were only plotted in cross-sections near the ADV measurement points, based on the blue particle trajectories

5 | RESULTS

5.1 | Bed changes and sediment size

Figures 2 and 3 illustrate the bed elevations and the grain size characteristics from sediment samples taken during the ADV measurement campaigns. Site A is located on the point bar and shows a mild slope from the deeper left side toward the bank on the right side of the oaks. The submerged and emergent oak fragments created local patchiness of smaller scour holes, sediment depositions and floating debris accumulations that further promoted the growth of macrophytes. On a larger scale, the fragmented oaks created global wake deposition of finer sediments downstream. The deposit is depicted by the bed contour of 62.0 m above datum, with the centre about 10 m downstream of the oak cluster (at x = 30.0 m, y = −7.0 m). The thickness of the accumulated sediments is up to 0.3 m, with a mean grain size decreasing to 2 mm.

At Site B, erosion and deposition patterns are more distinctly created by the individual trees. Scouring of the root bole and wake deposition are

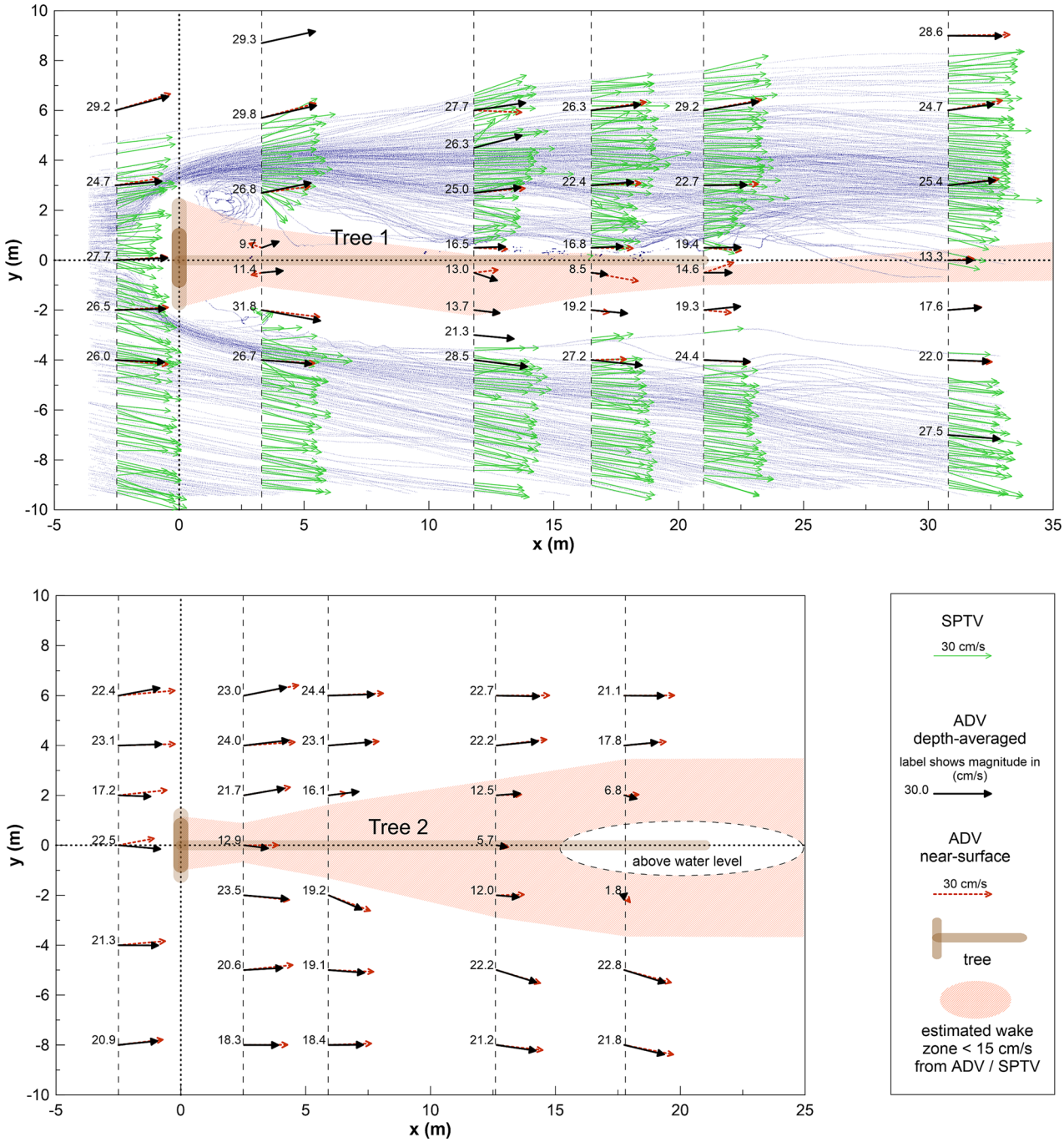

FIGURE 5 Vectors of horizontal mean flow velocity components (U, V) for Tree 1 and Tree 2 at Site B. Acoustic doppler velocimeter (ADV) points contain depth-averaged and near-surface vectors measured in 2019. Surface particle tracking velocimetry (SPTV) velocity vectors were only determined for Tree 1 and in cross-sections near the ADV measurement points, based on the blue particle trajectories. Note the increase in root bole diameter between the surveys in 2019 (ADV) and 2020 (SPTV)

evident for both trees. The upstream Tree 1 scoured down to 58.8 m above datum at the root bole and wake deposition extended up to 59.9 m. Referred to an average bed elevation of 59.4 m, this yields a relative scour depth of 0.6 m and a deposition height of 0.5 m. Relative scour depth was less for Tree 2 with 0.2 m, while the relative deposition was more pronounced with up to 0.9 m and slightly elevated above the water surface during the low flow conditions. With regard to grain sizes, the patterns are biased by a general trend of sediment fining from right to left in the cross-section of Site B. This may be attributed to the location and orientation of the trees in the river bend, with the point bar and finest sediments on the right side. However, in the wake deposits near the stem, the mean grain sizes are reduced to 2.0 mm compared with the surrounding sampling locations.

The grain size standard deviation σ also reduces in the wake deposits to values around 2.0 compared to an average of 4.0–5.0 in the surroundings. However, the standard deviation is a less characteristic

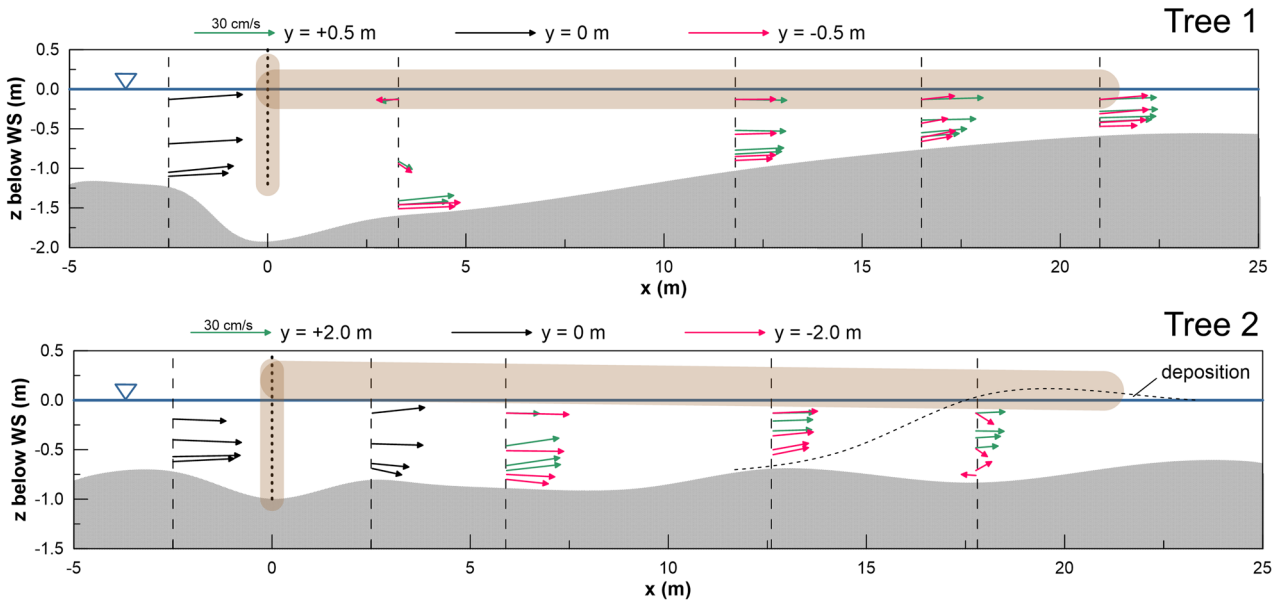

FIGURE 6 Streamwise-vertical velocity vectors (U, W) near the stem of Tree 1 and Tree 2 at Site B. Red vectors are located on the right, green vectors on the left side of the stem and black vectors in the centre. The bed topography contour shows the maximum scour in the centre and the wake deposit as indicated

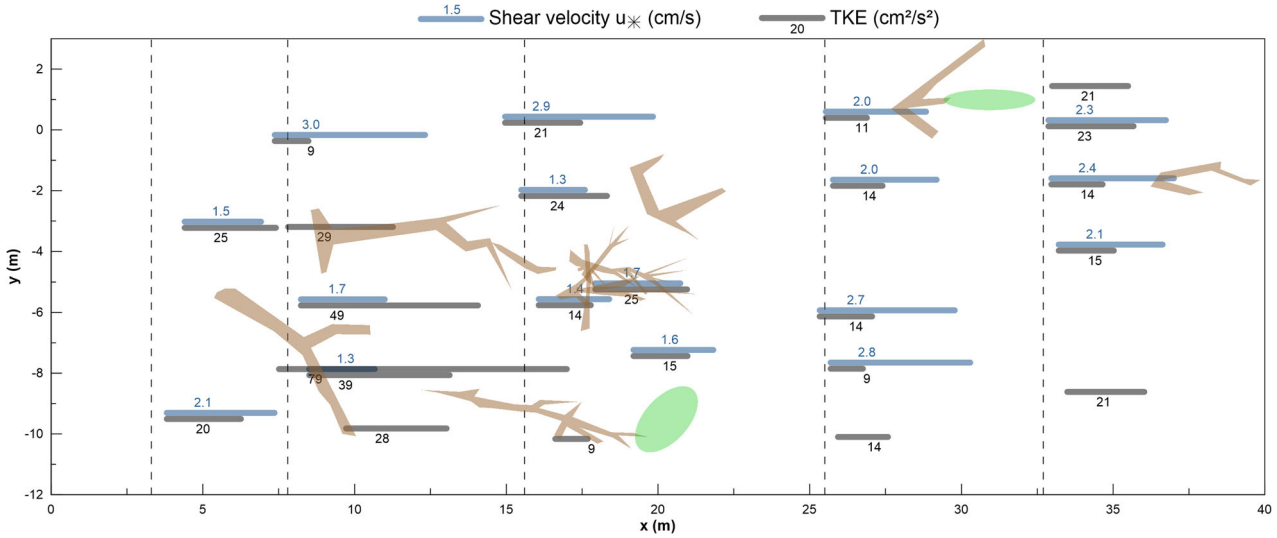

FIGURE 7 Depth-averaged turbulent kinetic energy (TKE) at Site A (grey bars) and shear velocity u_* (blue bars, missing bars indicate where boundary-layer analogies were not pronounced)

parameter for the Mulde due to a narrow bandwidth of grain sizes lacking larger gravel fractions (Vetter, 2019).

5.2 | Horizontal flow structure

At Site A, the SPTV method captured well the global flow patchiness created by the oak fragments (Figure 4). The SPTV-trajectories indicate smaller local wakes around individual fragments but also two superimposed wake structures around larger clusters. The smallest wakes scale with the immersed fragment size or diameter, which is in the order of magnitude of a few decimetres. The two superimposed wakes downstream were 2.0 and 3.0 m wide and expanded 10 and 20 m downstream, thus significantly larger than local wakes. ADV measurements were too widely spaced for capturing the horizontal flow structure on the patch scale but served as a valuable validation for the SPTV data—showing a good agreement between both methods.

At Site B, the flow separated from the edges of the root boles and created large wake zones near the stems (Figure 5). A slight asymmetry between the left and the right side of the wakes is observed. At the right side, flow divergence and contraction around the root bole edge locally increased the flow velocity (Tree 1: 31.8 cm/s, Tree 2: 23.5 cm/s). On the

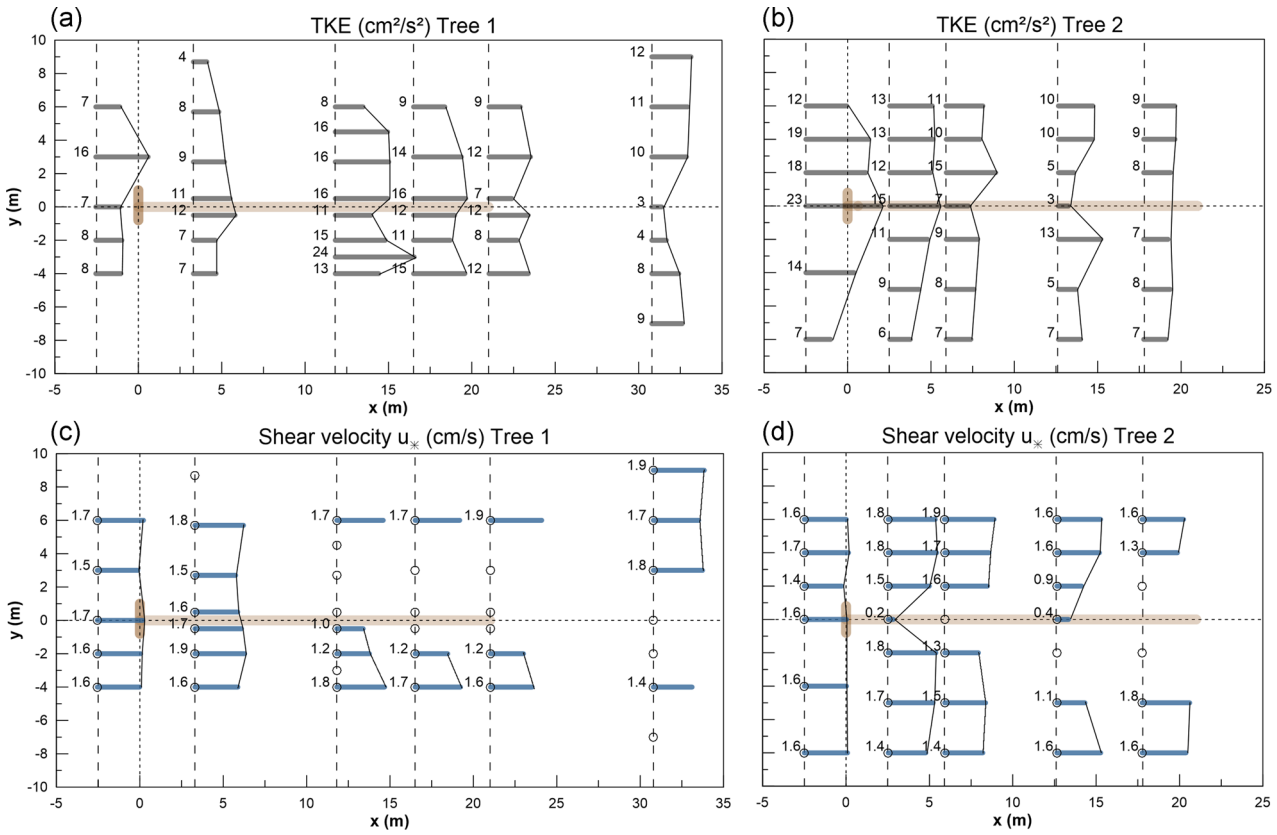

FIGURE 8 Trees 1 and 2 at Site B; (a) depth-averaged turbulent kinetic energy (TKE) (b) shear velocity u_* determined from wall-boundary layer analogies (not possible at all locations)

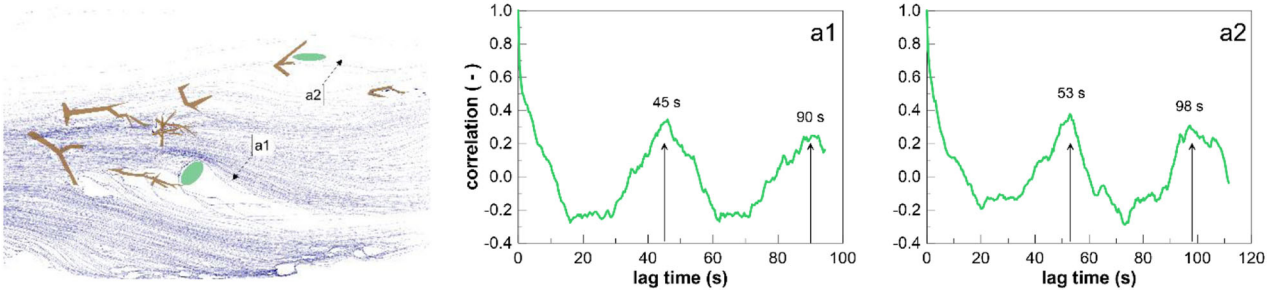

FIGURE 9 Correlation plots of transverse velocity components at two locations, 'a1' and 'a2', at Site A

left side, the angle of the flow divergence away from the trees was larger and the local flow acceleration less pronounced. More details are revealed by the SPTV trajectories around Tree 1 that show no interaction between the left and right shear layers, separated by the tree stem. On the left side of Tree 1, a smaller recirculation cell was established and particles were advected inward following undulating trajectories downstream. On the right side, trajectories were straight. Nevertheless, a recirculation on the right side was also present but not covered by the floaters during the SPTV.

The approaching flow was centrally diverted underneath the root boles and through the scour holes, establishing an advective mean flow velocity of around 10.0 cm/s in the wake centre. This advection caused a reduction of the velocity difference across the shear layers and reduced the production of large-scale turbulence. The wakes of Tree 1 and Tree 2 were not overlapping due to the orientation and lateral offset of the tree stems with respect to the mean flow. Thus, the main differences between the flow around the two trees were the lower approach flow velocity and a more pronounced flow divergence for Tree 2. Both depend on the bed topography with a generally shallower flow depth and a wake deposit elevating above the water surface for Tree 2. This indicates that the raised bed levels due to the wake deposits of the upstream Tree 1 still affect the mean flow conditions of the downstream tree, even though the two wakes did not interfere in terms of turbulence.

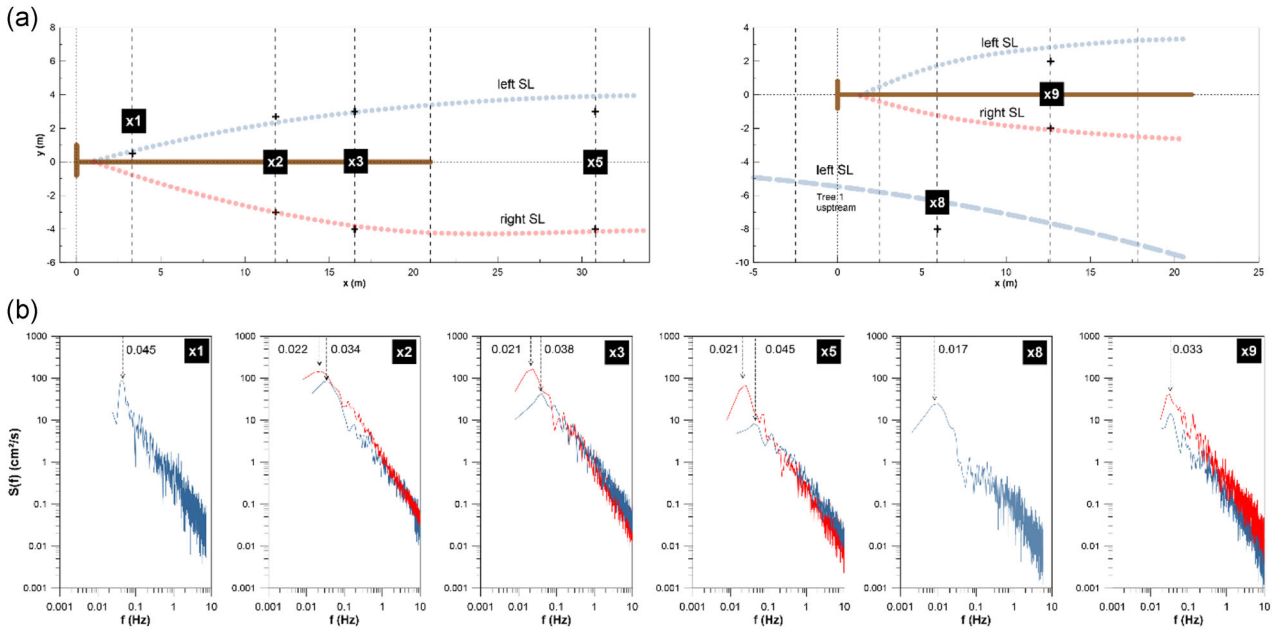

FIGURE 10 (a) Map showing the measurement locations with large-scale fluctuations identified from autocorrelation plots (+) around Trees 1 and 2 at Site B. Shear layer (SL) centrelines are indicated (blue = left SL, red = right SL). Note the different coordinate systems referenced to the tree axes of Tree 1 and Tree 2. (b) Autospectra of transverse velocity components in various cross-sections comprising spectra of left-sided SL (blue) and right-sided SL (red). Low-frequency peaks are indicated by arrows and the according to the dominant frequency

5.3 | Vertical flow structure near the root boles of Trees 1 and 2

Velocity vectors in the streamwise-vertical direction (u-w) measured with the ADVs add insight into the three-dimensional flow structure near the root boles at Site B (Figure 6). Tree 1 featured jet-like flow underneath the root bole through the scour hole, increasing the near-bed velocities as captured at location $x = 3.3$ m. At the same location, the flow reversed near the surface and on both sides of the stem. This indicates two smaller recirculation bubbles that occupied the top third of the water column. In contrast, Tree 2 neither features jet-like flow acceleration in the lower column nor flow reversal above at $x = 2.5$ m. The less pronounced scour hole and the stem partly emerged above the water surface and made a clear difference. Three-dimensionality in the flow structure was limited to the area around the root bole and the flow divergence around the wake deposit. Other than that, the wake flow pattern was more or less two-dimensional, dominated by bed friction. A similar dominance of bed friction occurred at Site A, where flow three-dimensionality was even smaller than at Site B and plots are, therefore, not included here.

5.4 | TKE and bed shear velocity

TKE (cm²/s²) is an integral parameter, accounting for turbulence produced by all present sources of shear. In contrast, shear velocity u_* (cm/s) relates, per definition, only to the bed shear. In Figures 7 and 8, distributions of both parameters are shown for Sites A and B, respectively.

Velocity and turbulence quantities followed the theoretical boundary layer distributions within at least the lower third of the water column in most verticals. This indicates the dominance of bed friction in this flow region. The shear velocities determined are uniformly distributed with average values and standard deviations of $u_* = 2.0 \pm 0.52$ cm/s (±26%) for the oaks at Site A, 1.61 ± 0.23 cm/s (±14%) for Tree 1 at Site B and 1.57 ± 0.18 cm/s (±11%) for Tree 2 at Site B. In comparison, the depth-averaged TKE values comprise larger local deviations: TKE = 22.5 ± 14.7 cm²/s² (±65%) for the oaks at Site A, 10.7 ± 4.0 cm/s (±38%) for Tree 1 at Site B and 10.3 ± 4.2 cm/s (±41%) for Tree 2 at Site B, respectively. This relates to shear layer generated turbulence that also increases small-scale turbulence but does not affect the bed shear to a larger extent.

5.5 | Large-scale turbulence induced by the wood structures

Autocorrelation plots of the measured ADV velocities gave insight into the growth and coherence of shear layers and large-scale turbulence. At Site A, large-scale fluctuations occurred at two locations (marked 'a1' and 'a2' in Figure 9). The locations are downstream of the oak cluster and laterally separated by a distance of 12 m. The dominant periods in the transverse velocity component, depicted by consecutive peaks in the autocorrelation lag-plots, were between $t_e = f_e^{-1} =$ 45 s (a1) and 45–53 s (a2).

The ADV measurements at Site B were longer and low-frequency peaks associated with large-scale turbulence were extracted directly from the autocorrelation spectra. Such peaks occurred in the left and

right shear layers of both trees at Site B (Figure 10). The right-sided shear layer of Tree 1 has a dominant period of approximately t_e = 48 s ($f_e = t_e^{-1}$ = 0.021 Hz), the left-sided shear layer of 25 s (0.034–0.045 Hz). The left shear layer persists for a downstream distance of at least 60 m, indicated by a dominant period of t_e = 59 s (0.017 Hz) at location '×8' far to the right of Tree 2. For Tree 2, the left and right-sided shear layers are more symmetric with a period of t_e = 30 s (0.033 Hz) on both sides.

5.6 | Application of the shear layer model equations

For the fragmented oaks at Site A, the identification of shear layers is not easily possible because of the coarse ADV measurement grid. SPTV trajectories indicate that the tree fragments were too heterogeneously distributed to merge into a single superimposed wake structure (Figure 4). Instead, several smaller and separated wake zones of a width of 2–3 m were established. Equation (4) applied to a mean velocity of U_0 = 30 cm/s and a dominant frequency of f_e = 0.02 Hz identified at the two locations 'a1' and 'a2' (Figure 9) yields Strouhal numbers of St = 0.13–0.2. These values are near 0.2 as proposed for porous wakes by Zong and Nepf (2012), despite the lower Reynolds numbers in their lab experiments.

At Site B, the denser data coverage allows applying the shear layer model Equations (1)–(3). First, Equation (1) yields a maximum wake length scale L_{KV} = 16 m downstream of Tree 1, respectively 9 m downstream of Tree 2 (Table 1). Application of Equation (2) yields the evolution of the shear layer width, taking into account the bed friction as a destabilizing mechanism. In Figure 11, the shear layer centreline is aligned with the mean flow pattern and half of the calculated shear layer width from Equation (2) is added toward each side to identify the shear layer margins. Two additional parameters were used to confirm the shear layer evolution as shown in Figure 11: first, the shear layer widths reasonably coincide with the sign and magnitude of the measured maximum lateral turbulent stresses = $u'v'_{max}$ in each vertical (indicated in Figure 11, when colours of the shear layers and stresses are matching). Further, the dominant periods predicted with Equation (3) reasonably match the measured (Table 1). Therefore, the shear layers originating from the root boles at Site B remain separated for a distance much longer than the wake length scale and, thus, differ from idealised porous wake configurations of vertical cylinders.

6 | DISCUSSION

Field measurements in this study were conducted during low flows, resulting in low mean flow velocities, weak velocity gradients and turbulence production. In general, the flow was dominated by vertical shear due to bed friction as the main contribution to turbulent stresses and TKE. Horizontal shear layers originated from flow separation at the edges of the wood structures and locally increased the levels of turbulent stresses and TKE. Nevertheless, this increase was less than

TABLE 1 Shear layer (SL) properties of Tree 1 and 2 at Site B from the measured data, calculations and predictions with the SL model Equations (1–3)

Tree	SL side	Initial velocity difference ADV data ΔU_0 (cm/s)	Initial centreline velocity ADV data U_{c0} (cm/s)	Bed friction coefficient calculated c_f (–)	Water depth measured h (m)	Initial SL width set δ_0 (m)	Wake lenth scale Equation (1) with D = 2 m L_{KV} (m)	Relative coordinate set x' (m)	SL width Equation (2) $\delta(x')$ (m)	SL dominant frequency Equation (3) $f_e(x')$ (Hz)	SL dominant frequency Measured $f_e(x')$ (Hz)
1	Left	20	20	0.0128	1.6	0.6	9.1	11.8	1.7	0.034	0.034
								51.7	3.6	0.016	0.017
	Right	20	20	0.0128	1.5	0.8	9.1	11.8	2.0	0.029	0.021
2	Left	11	18	0.0128	0.6	0.7	14.9	12.6	1.4	0.032	0.033
	Right	10	18	0.0128	0.6	0.7	16.4	12.6	1.3	0.033	0.033

Note: Constant values were taken for the spreading coefficient α = 0.11, scaling coefficient λ = 0.5 and the Strouhal-number St = 0.2.
Abbreviations: ADV, acoustic Doppler velocimeter; SL, shear layer.

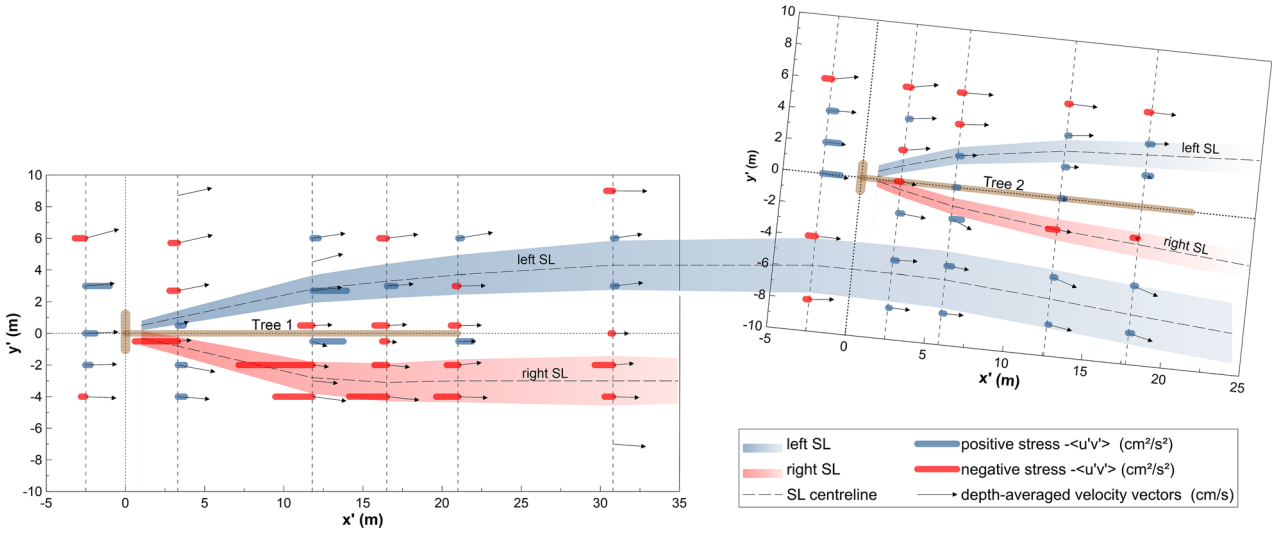

FIGURE 11 Local shear layer (SL) widths and periods predicted with the analytical SL model for Trees 1 and 2 at Site B. Depth-averaged velocity vectors were used for fitting the SL centrelines in the measured cross-sections. Negative stresses (red) coincide with anti-clockwise rotation (right-sided SLs), positive stresses (blue) with clockwise rotation (left-sided SLs). The maximum stresses in each vertical were used, mostly at around two-thirds of the water column

expected due to the flow permeability of the wood structures that decreased the lateral velocity gradients across the wakes.

Flow permeability in the case of the natural oaks at Site A was controlled by the porosity due to the wood fragmentation. With porosities above 85%, the fragmented oaks were classified into the highly porous regime in the literature (Zong & Nepf, 2012), where not all analogies with idealised lab configurations may hold anymore.

At Site B, trees composed of a solid root bole and a long stem were installed. Hereby, flow permeability through the structure was provided by scouring, vertical flow diversion into the scour hole and farther into the wake. Analyses revealed that the shear layers originating from the outermost edges of the root boles remained separated and did not interact to form a vortex street pattern. Two mechanisms contribute to the persistent shear layer separation: (i) the tree stem and the wake sediment deposits acting as a physical flow barrier and disconnecting the shear layers, similar to wake-splitter plates (Apelt & West, 1975; Schnauder & Moggridge, 2009) and (ii) the bed friction limiting the lateral growth of the shear layers.

As expected, morphological changes are an important adaptation mechanism to flow modifications induced by wood structures in rivers. Wood installations are possible anywhere in a river cross-section and, thus, provide a high potential for morphological adaptation processes, with all the benefits for ecology. One open question remains in this context that has implications for the optimum design of wood structures in river engineering: how will flow and morphology change at higher discharges?

It may be hypothesized that higher discharges result in larger lateral velocity gradients and, thus, in more pronounced shear layers. For the fragmented oaks, higher discharges and the rise of the water level would cause submergence and, thus, a shift from two-dimensional shallow wake characteristics to three-dimensional wake bubbles (e.g., Ouro et al., 2017). For the installed trees, higher discharges would probably suspend the entire structure from the bed due to its buoyancy. This detachment from the bed may cause substantial changes in the scouring and bed morphology. A submerged wall jet flow pattern established with maximum bed shear shifted further downstream (e.g., Sumer et al., 1988). The root bole scour holes are likely to level out under such conditions and scouring as well as subsequent depositions would occur further downstream. The presence of a stem is likely to have less effect during detached conditions. Typically, a wake bubble would establish near the surface with pronounced three-dimensionality of the flow (e.g., Norman & McKeon, 2012). The dominance of horizontal shear layers typical for shallow flows would, thus, diminish and with it, potential wake-splitter effects.

In summary, the present study provided a useful methodology to investigate and analyse the flow and morphology of wood structures in rivers. The compiled analytical models are valuable for the quantification and localisation of the different flow habitats provided by wood-induced wakes. However, the transitions from a wall boundary layer to a shallow or deep wake flow, once the wood is inserted, are complex and come along with morphological adaptations on different scales. Studying the interplay between these factors is a major task for ecohydraulic research. It will be the key to allowing more wood in our rivers, maximising ecological benefits and minimising the risks for infrastructure and flooding.

ACKNOWLEDGEMENTS

Assistance during the demanding field campaigns is thankfully acknowledged; Christoph Lehmann (Gerstgraser), Manuela König (TUBS), Jakob Höllrigl (TU Wien) and Haike Weichel. Stan Thorez (TU

Wien) helped with MATLAB programming for PTV analyses. The 'Wilde Mulde' project was jointly funded by the Federal Ministry of Education and Research (BMBF) and the Federal Agency for Nature Conservation (BfN) with funds also from the Federal Ministry for the Environment, Nature Conservation and Nuclear Safety (BMU) in Germany (funding code: 01LC1322F). Additional funds for the campaigns 2019/2020 were provided by TU Wien (Institute of Hydraulic Engineering and Water Resources Management) and TU Wien Bibliothek (Open Access Funding Programme). The two reviewers are thanked for their efforts in improving the manuscript in a positive and supportive way.

ORCID

Ingo Schnauder https://orcid.org/0000-0002-9608-758X
Christine Anlanger http://orcid.org/0000-0001-6666-422X
Katinka Koll http://orcid.org/0000-0003-3026-4085

REFERENCES

Anlanger, C., Attermeyer, K., Hille, S., Kamjunke, N., Koll, K., König, M., Schnauder, I., Nogueira Tavares, C., Weitere, M., & Brauns, M. (2022). Large wood in river restoration: effects on hydromorphology, biodiversity and ecosystem functioning. *International Review of Hydrobiology*. Manuscript submitted for publication.

Apelt, C. J., & West, G. S. (1975). The effects of wake splitter plates on bluff-body flow in the range $10^4 < R < 5 \times 10^4$. Part 2. *Journal of Fluid Mechanics*, *71*, 145–160.

Chang, K., & Constantinescu, G. (2015). Numerical investigation of flow and turbulence structure through and around a circular array of rigid cylinders. *Journal of Fluid Mechanics*, *776*, 161–199. https://doi.org/10.1017/jfm.2015.321

Chu, V. H., & Babarutsi, S. (1988). Confinement and bed-friction effects in shallow turbulent mixing layers. *Journal of Hydraulic Engineering*, *114*, 1257–1274.

Edwards, P. J., Kollmann, J., Gurnell, A. M., Petts, G. E., Tockner, K., & Ward, J. V. (1999). A conceptual model of vegetation dynamics on gravel bars of a large Alpine river. *Wetland Ecology Management*, *7*, 141–153.

Gippel, C. J., O'Neill, I. C., Finlayson, B. L., & Schnatz, I. (1996). Hydraulic guidelines for the re-introduction and management of large woody debris in lowland rivers. *Regulated Rivers: Research and Management*, *12*, 223–236.

Gurnell, A. M., Petts, G. E., Harris, N., Ward, J. V., Tockner, K., Edwards, P. J., & Kollmann, J. (2000). Large wood retention in river channels: The case of the Fiume Tagliamento, Italy. *Earth Surface Processes and Landforms*, *25*(3), 255–275.

Gurnell, A. M., Piégay, H., Swanson, F. J., & Gregory, S. V. (2002). Large wood and fluvial processes. *Freshwater Biology*, *47*, 601–619. https://doi.org/10.1046/j.1365-2427.2002.00916.x

Heyman, J. (2019). TracTrac: A fast multi-object tracking algorithm for motion estimation. *Computers & Geosciences*, *128*, 11–18. https://doi.org/10.1016/j.cageo.2019.03.007

Nezu, I., & Nakagawa, H. (1993). Turbulence in open-channel flows, *IAHR monograph*. Balkema.

Nicolle, A., & Eames, I. (2011). Numerical study of flow through and around a circular array of cylinders. *Journal of Fluid Mechanics*, *1*(1), 1–31.

Norman, A. K., & McKeon, B. J. (2012, June 23–26). *Effect of sting size on the wake of a sphere at subcritical Reynolds numbers*, 38th Fluid Dynamics Conference and Exhibit. American Institute of Aeronautics and Astronautics, Seattle, WA. https://doi.org/10.2514/6.2008-4183

Ouro P., Wilson C. A. M. E., Evans P., & Angeloudis A. (2017). Large-eddy simulation of shallow turbulent wakes behind a conical island. *Physics of Fluids*, *29*(12), 126601. http://doi.org/10.1063/1.5004028

Prinz, F., Brevis, W., & Socolofsky, S. (2012, June 4–6). *Shallow wake formed after porous structures: charaterisation of the influence of the solid volume fraction*. Proceedings 3rd International Symposium on Shallow Flows (ISSF), University of Iowa, Iowa City, IA.

Van Prooijen, B. C. (2004). Shallow mixing layers [PhD thesis, Delft University of Technology, Delft, Netherlands]. https://repository.tudelft.nl/islandora/object/uuid%3A8eec05c0-73cf-4284-9439-c0246cddf160

Schnauder, I., & Moggridge, H. L. (2009). Vegetation and hydraulic-morphological interactions at the individual plant, patch and channel scale. *Aquatic Sciences*, *71*, 318–330. https://doi.org/10.1007/s00027-009-9202-6

Schnauder, I., Yagci, O., & Sedat, K. (2007). The effect of permeability of natural emergent vegetation on flow velocity and turbulence, *Proceedings of the 32nd International Congress of IAHR*. IAHR.

Schulz-Zunkel, C., Anlanger, C., Baborowski, M., Bondar-Kunze, E., Brauns, M., Gapinski, C., Gründling, R., von Haaren, C., Hein, T., Henle, K., Junge, F., Kasperidus, H. D., Koll, K., Kretz, L., Rast, G., Schnauder, I., Scholz, M., Schrenner, H., Seele-Dilbat, C., … Dziock, F. (2022). Effective restoration measures in river-floodplain ecosystems—The 'Wilde Mulde' project. *International Review of Hydrobiology*. Manuscript submitted for publication.

Sukhodolov, A. N., Schnauder, I., & Uijttewaal, W. S. J. (2010). Dynamics of shallow lateral shear layers: Experimental study in a river with a sandy bed. *Water Resources Research*, *46*(11), 1–18. https://doi.org/10.1029/2010WR009245

Sukhodolov, A., Thiele, M., & Bungartz, H. (1998). Turbulence structure in a river reach with sand bed. *Water Resources Research*, *34*(5), 1317–1334.

Sumer, B. M., Jensen, H. R., Mao, Y., & Fredsoe, J. (1988). Effect of lee-wake on scour below pipelines in current. *Journal of Waterway, Port, Coastal, and Ocean Engineering*, *114*, 599–614.

Takemura, T., & Tanaka, N. (2007). Flow structures and drag characteristics of a colony-type emergent roughness model mounted on a flat plate in uniform flow. *Fluid Dynamics Research*, *39*, 694–710.

Uijttewaal, W. S. J., & Booij, R. (2000). Effects of shallowness on the development of free-surface mixing layers. *Physics of Fluids*, *12*, 392–402.

Vetter, T. (2019). Sohlmorphologie und Hochwassermorphodynamik eines Flachlandflusses mit Geschiebegleichgewicht und -defizit. *Korrespondenz WaWi*, *19*(5), 287–295.

Zong, L., & Nepf, H. (2012). Vortex development behind a finite porous obstruction in a channel. *Journal of Fluid Mechanics*, *691*, 368–391. https://doi.org/10.1017/jfm.2011.479

SUPPORTING INFORMATION

Additional supporting information may be found in the online version of the article at the publisher's website.

How to cite this article: Schnauder, I., Anlanger, C., & Koll, K. (2022). Wake flow patterns and turbulence around naturally deposited and installed trees in a gravel bed river. *International Review of Hydrobiology*, 107, 22–33. https://doi.org/10.1002/iroh.202102096